Determination of permeability using a classic Darcy water column

Fabian B. Wadsworth, Caron E. J. Vossen, Diana Schmid, Mathieu Colombier, Michael J. Heap, Bettina Scheu, and Donald B. Dingwell

Citation: American Journal of Physics **88**, 20 (2020); doi: 10.1119/10.0000296

View online: https://doi.org/10.1119/10.0000296

View Table of Contents: https://aapt.scitation.org/toc/ajp/88/1

Published by the American Association of Physics Teachers

Determination of permeability using a classic Darcy water column

Fabian B. Wadsworth[a)]
Earth Sciences, Durham University, Durham DH1 3LE, United Kingdom

Caron E. J. Vossen, Diana Schmid, and Mathieu Colombier
Earth and Environmental Sciences, Ludwig-Maximilians-Universität, Munich 80333, Germany

Michael J. Heap
Geophysique Expérimentale, Institut de Physique de Globe de Strasbourg (UMR 7516 CNRS, Université de Strasbourg), 5 rue René Descartes, 67084 Strasbourg, France

Bettina Scheu and Donald B. Dingwell
Earth and Environmental Sciences, Ludwig-Maximilians-Universität, Munich 80333, Germany

(Received 28 August 2019; accepted 12 November 2019)

Permeability is a macroscopic property of materials with a percolating pore phase, such as many rocks and filters. We describe a simple experiment for the empirical determination of permeability using a low-cost method similar to that used by Darcy. We advocate the use of controlled cylindrical sintered filters, for which there is theoretical constraint of the permeability as a function of porosity, against which empirical results can be compared. The methodology presented here provides a step-by-step approach to laboratory experiments and numerical techniques for fitting a linear equation to data and is appropriate for undergraduate Physics, Earth Science, or Engineering courses.
https://doi.org/10.1119/10.0000296

I. STATEMENT OF THE PROBLEM

Permeability is an intrinsic physical property of porous solids and represents how efficiently a material can transmit fluids. In both natural and industrial permeable materials, this property can vary by many orders of magnitude. A classic example is to imagine a tube full of stationary sand grains through which water is flowing; the permeability value is essentially a measure of how much the sand and the tube walls resist the fluid flow. Darcy's law[1] uses this material property of permeability as a coefficient to relate the pressure drop across the material length to the average speed of the fluid $\langle u \rangle$ through the material,

$$\nabla P = -\frac{\mu}{k}\langle u \rangle, \tag{1}$$

where μ is the dynamic viscosity of the fluid (dimensions $[\mathrm{M}][\mathrm{L}]^{-1}[\mathrm{T}]^{-1}$), k is the permeability (dimensions $[\mathrm{L}]^2$), and ∇P is the pressure drop over a given length (dimensions $[\mathrm{M}][\mathrm{L}]^{-2}[\mathrm{T}]^{-2}$). Here, we have used the notation from dimensional analysis, where $[\mathrm{L}]$ represents the length, $[\mathrm{M}]$ represents the mass, and $[\mathrm{T}]$ represents the time.

The Reynolds number defines whether a flow is influenced by inertia in the fluid or not and is $\mathrm{Re} = \rho u Z/\mu$, where ρ is the fluid density (dimensions $[\mathrm{M}][\mathrm{L}]^{-3}$), u is the local fluid velocity, and Z is a lengthscale relevant to the flow. Equation (1) is valid in the low Reynolds number regime only.[2] Forchheimer's equation[3] extends Darcy's law (Eq. (1)) to a high Reynolds number

$$\nabla P = -\frac{\mu}{k}\langle u \rangle - \frac{\rho}{k_\mathrm{I}}\langle u \rangle^2, \tag{2}$$

where k_I is a second coefficient for this problem, usually referred to as the inertial permeability (dimensions $[\mathrm{L}]$). Equation (2) allows us to define the lengthscale Z in the problem of flow through porous media as $Z = k/k_\mathrm{I}$.

A student could easily plot the result of both Eqs. (1) and (2) for the same range of inputs over a wide range of $\langle u \rangle$ to see visually that Eq. (1) is the low flow speed linear limit of Eq. (2). In Fig. 1, we provide an example of such a plot to demonstrate that Eq. (1) is a limiting solution of Eq. (2) at low values of ∇P for some realistic inputs for the fluid properties $\mu = 10^{-3}$ Pa s and $\rho = 1000\,\mathrm{kg\ m^{-3}}$ (typical values for water at 20 °C) and for the solid properties of $k = 10^{-12}\,\mathrm{m^2}$ and $k_\mathrm{I} = 10^{-8}$ m (typical values for sintered solids used here; see Sec. IV). Using $\langle u \rangle$ in place of u in the Reynolds number given above and the lengthscale Z defined as the ratio of the viscous and inertial permeabilities, a student could add to Fig. 1 and find graphically that, indeed, the solution to Eqs. (1) and (2) converges at $\mathrm{Re} \ll 1$.

In this contribution, we confine ourselves to the low Reynolds number regime in which Eq. (1) is valid and in which the second term on the right-hand side of Eq. (2) is effectively zero. In that situation, there is a useful opportunity for students at a wide range of levels to explore the rigorous work-flow involved in making experimental measurements and performing data analysis to extract a single unknown material property, k. Equation (2) provides an additional opportunity for more students at higher levels to extend the same work-flow to non-linear problems.

Given that models for k generally exist only for idealized internal geometries in porous media,[4–6] the toolkit used to constrain permeability using empirical measurement remains a mainstay of many engineering or applied disciplines. Therefore, it can be an engaging student practical in a classroom environment and offers a variety of opportunities for developing experience in data analysis, simple numerical techniques using code, mathematics of scaling or dimensional analysis, and careful experimental practice, as well as developing intuitions for general fluid flow problems.

II. MOTIVATION

The permeability of materials is of fundamental importance in many physical science disciplines. In engineering topics of study, permeability controls the rates at which gas

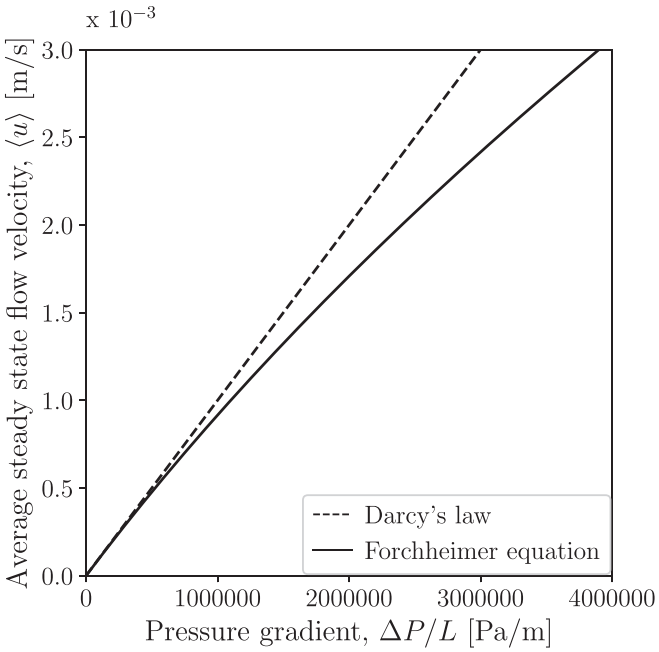

Fig. 1. An example solution to Darcy's law (Eq. (1)) and Forchheimer's equation (Eq. (2)) for a specific set of input values, $\mu = 10^{-3}$ Pa s, $\rho = 1000\,\mathrm{kg\,m^{-3}}$, $k = 10^{-12}\mathrm{m}^2$, and $k_I = 10^{-8}$ m. This shows that Darcy's law is the low $\langle u\rangle$, low $\Delta P/L$ limit for Forchheimer's equation. We note that the pressure gradient $\nabla P \approx \Delta P/L$ for small isotropic systems, such as are the focus of this contribution.

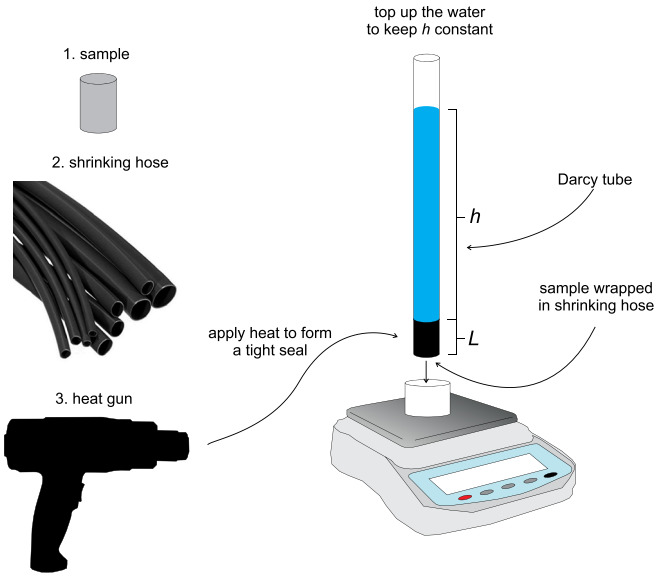

Fig. 2. The experimental set up. The black section at the base of the plastic water-filled tube is the sample-in-shrinking-hose array. The shrinking hose is made tight against the sample and the tube by using the heat gun.

or liquid moves through particle filters designed to scrub toxins from the flow.[7] In Earth sciences, permeability controls the migration and fluid pressures of hydrocarbons and water in the Earth's porous upper crust, as well as the rates at which pressurized gas is released from active volcanoes.[8] In the sub-millimeter flows (called microfluidics), permeability controls the small-scale movement of fluids through porous networks.[9] In the preparation of coffee, permeability of the ground coffee pack determines the contact time between hot fluids and the coffee itself.[10] And, more generally, there are analogies between permeable flow through porous media and the movement along electric circuits.[9]

In Earth sciences, in particular, students often arrive at undergraduate levels without experience of data analysis, dimensional analysis, or experimental methods.[11] While this is not necessarily a problem because the geosciences have a range of learning outcomes, not all of which demand strong quantitative skills, it is possible that weaknesses in data-based work such as shown here could hold students back.[12] We propose that this exercise could be a useful addition to many existing engineering, Earth sciences and geography curricula at the early undergraduate level or as part of high school (secondary education) physics or geography courses, and that this is an engaging example of how instructors can lead students from problem statement, through hypothesis testing, and to theoretical and empirical results at extremely low-cost.

III. EXPERIMENTAL DESIGN: THE DARCY COLUMN

We choose to use an experimental setup similar to the classic Darcy design, which is composed of a column containing water at the base of which sits a permeable sample or material (Fig. 2). The column is made of a 2 m long, 2 cm inner diameter, transparent plastic tube. The tube should be marked with a vertical scale using a pen that can write on the plastic. We recommend that the scale is marked at least at every 2 cm, starting from zero at the point where the top of the sample will sit. We use cylindrical coherent samples (see Sec. III) of the same diameter as the inner diameter of the tube. (The sample must be a snug fit to the tube or the measurement will be less accurate.) We position the samples such that they are half in the bottom opening of the tube and half overhanging the bottom of the tube. We then wrap a shrinking hose material around the outside of the tube and the overhanging part of the sample. The shrinking hose is heated with a heat gun to activate the shrinking hose, which forms a tight seal around both the sample and the tube. If the shrinking hose extends the full length of the sample, but does not overhang the bottom of the sample, this produces a system in which the sample is simply the basal plug to the tube but where the water can flow freely through the sample.

Once the sample-tube assembly is constructed, we clamp this on a laboratory stand so that it is vertical and we fill the tube with water to a known height above the top of the sample. The weight of the water that overlies the sample confers a pressure head, which drives flow of the water through the permeable sample. We place a container on a calibrated mass balance (accurate to 0.01 g) beneath the sample so that the outflow of water drips into the container and its mass can be measured during the experiment. It is crucial that the level of the water in the tube above the sample is topped up constantly so that the pressure head can be considered constant. For some samples with a high permeability, this procedure of topping up the sample will be more challenging because the flow out of the tube will be rapid. This setup is low-cost (plastic tubing, shrinking hose, container, and balance) and easy to build and deconstruct when it is not in use.

The variables we measure are (1) the mass of water exiting the sample as a function of time $\dot{m}$(with dimensions $[\mathrm{M}][\mathrm{T}]^{-1}$) and (2) the water level height relative to the top of the sample (including a measure of how variable this level was).

IV. SAMPLE MATERIALS

There are many different porous material types that could be selected for testing in a classroom using the methods proposed herein. We choose to use sintered cylindrical samples with defined dimensions and porosity. These can be made in a custom manner, or they are available commercially (e.g., via AmesPore® https://amespore.com/en/). We use a 2 cm diameter sample with a 4 cm length. Samples smaller than this will prove more challenging to measure.

We use sintered samples because there is a rigorous theoretical framework for their hydraulic properties[13] (see Sec. VI) and because they are simple and low-cost to manufacture. We note that this is not essential, because it requires specialist equipment (a furnace, large ceramic trays, and a pillar drill with a sturdy coring diamond-tipped drill bit), and that commercially available ready-sintered filters would also be appropriate. Nevertheless, we describe below the method for creating sintered samples for this exercise.

We use Spheriglass® glass particles available from Potters Industries™ with monodisperse radius $\langle R \rangle = 9.41 \times 10^{-5}$ m as a starting material. We pour them loosely into an AL24 alumina ceramic tray from Friatec GmbH (Germany), scraping the top until a flat, but not compacted bed of beads is created. We then place the tray in a Hereus™ furnace and heat it at 10 K min^{-1} to 900 K for different hold-times before cooling at 10 K min^{-1} back to room temperature, rotating the tray 180 °, and heating back to 900 K for the same hold time. For a specific temperature and glass bead size and composition, the hold time controls the resultant porosity, such that longer hold times will result in lower porosity samples.[14] As an example, we used $10 - 60$ h total hold times to reach porosities in the range given here. If a higher temperature is used, then the hold times required to reach the same porosities will be lower.

This method of using a relatively low isothermal temperature and rotating the tray halfway through ensures a sintered block that is approximately homogeneous. We then tip the sintered block out of the tray, and turn it on its end to drill cylindrical cores sideways from the block using a 20 mm inner diameter coring drill-bit with a diamond-tipped edge in a pillar drill. The resulting long cylinders are then cut to length using a circular saw and the ends polished flat and plane-parallel. In Fig. 3, we show a cartoon of this entire sample-preparation technique and how it relates to the experimental set up as a whole.

We measured the porosity of each sample using a simple method. First, the mass m_s and volume V_s of the cylinder is measured (where V_s can be determined using the cylindrical radius $d/2$, where d is the cylindrical diameter, and length L measured using calipers). This permits us to compute the bulk density of the sample $\rho_s = m_s/V_s$. The samples are composed of two phases, a solid glass bead phase with density ρ_g (in this case, $\rho_g = 2500\,\text{kg m}^{-3}$) and air in the pore phase with density ρ_a. It is clear that because the air occupies some of the volume of the sample, then $\rho_s < \rho_g$. If we take ρ_a to be negligibly small compared with ρ_g, the total porosity of the samples is simply $\phi = 1 - \rho_s/\rho_g$. Sintered samples such as these do not have a measurable fraction of isolated porosity.[13]

V. WORK-FLOW AND EXAMPLE RESULTS

Here, we provide an example workflow and an example dataset (available in full in the supplementary material)[23] to demonstrate the procedure we are proposing. The output from the experimental design given above is $\dot{m}$ as a function of time t and of the height of the water above the sample top in the tube h. Using the following work-flow, we can convert $\dot{m}$ to $\langle u \rangle$ and h to ∇P, which both are the parameters needed in Eq. (1).

We collected measurements of $\dot{m}$ as a function of time for a single water height h, before repeating for another h (where the measurement of h is facilitated by the scale drawn on the tube). In Fig. 4(a), we show two examples of such time series data. In our case, the data are at a steady state, such that we can take the mean of the data (dashed line in Fig. 4(a)) and a standard deviation σ about the mean (the 2 σ range about the mean given by the grey bar in Fig. 4(a)). In other cases (especially for low permeability samples), a transient non-steady-state portion of these data may be measurable, and should be discarded prior to further analysis.

We convert $\dot{m}$ to $\langle u \rangle$ via $\langle u \rangle = Q/A = \dot{m}/(\rho A)$, where A is the cross sectional area of the sample (with dimensions

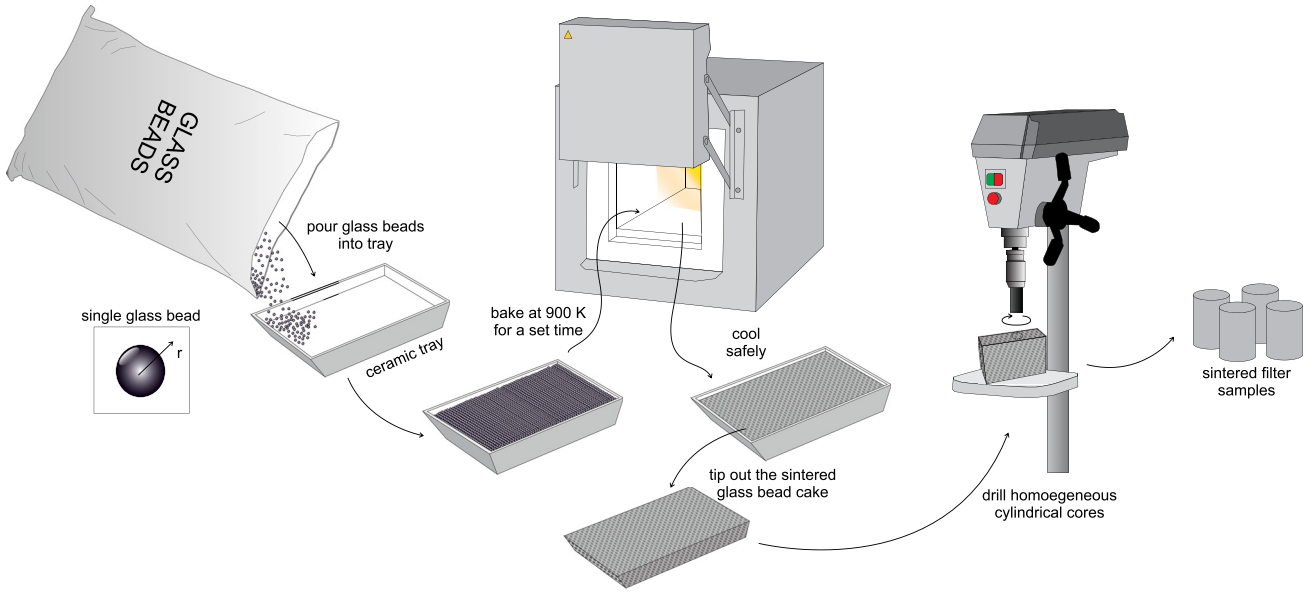

Fig. 3. Optional sample preparation method to create reproducible permeable filter cylinders. See text for details.

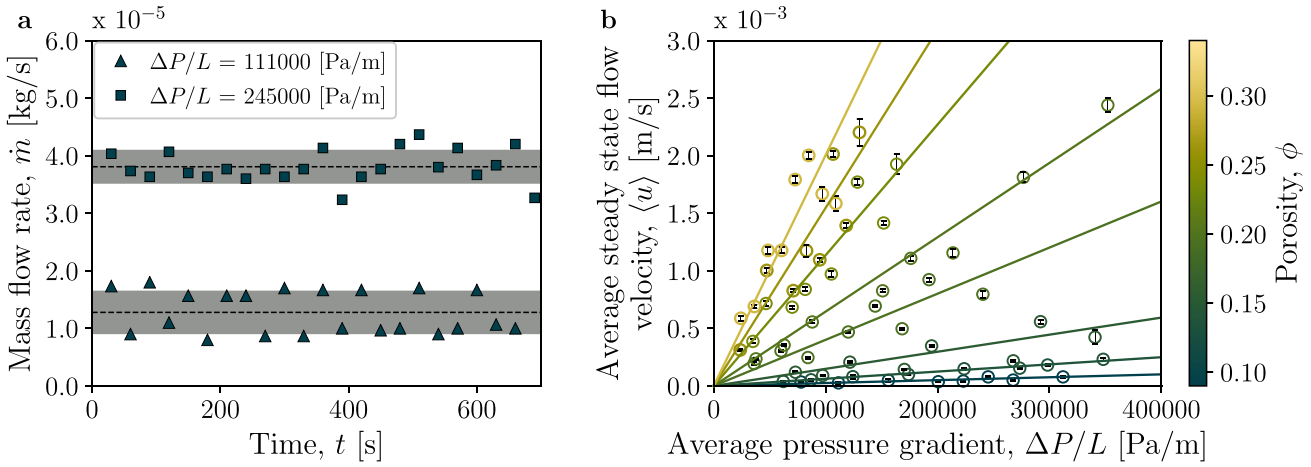

Fig. 4. Raw data. (a) Mass flow rate $\dot{m}$ as a function of time t shown for two example values of driving pressure gradient $\Delta P/L$. The dashed line represents the steady-state average value of $\dot{m}$, and the grey bar represents the range of values for $\dot{m}$ that are within 1σ of that mean (such that the grey bar has vertical thickness 2σ). (b) Average steady-state flow speed $\langle u \rangle$ as a function of the applied average driving pressure gradient $\Delta P/L$ with curves fit to each dataset using Eq. (3) for which k is the only unknown fit parameter. The error bars on $\langle u \rangle$ are dominated by the uncertainty on the raw $\dot{m}$ [examples given in panel (a)]. The colour map for porosity in (b) is from Fabio Crameri (Ref. 21) and is designed to be perceptually uniform, colour-vision-deficiency friendly, and readable as black-and-white print.

$[\mathrm{L}]^2$) and Q is a volume flux of water (with dimensions $[\mathrm{L}]^3[\mathrm{T}]^{-1}$). The uncertainty on $\langle u \rangle$ can be related to the standard deviation (Fig. 4(a)), via the standard error $\epsilon = \sigma/\sqrt{n}$, where n is the number of data points used for computing the mean. This error is also converted to units consistent with $\langle u \rangle$ using the above conversion, and then used to plot error bars for each $\langle u \rangle$ (Fig. 4(b)).

Over small length scales and for isotropic samples, ∇P can be approximated as $\Delta P/L$, and ΔP is the difference between the pressure on the top of the sample P_1 and the pressure beneath the sample P_2. The first pressure (or upstream pressure) P_1 is related to the height of the water in the tube h, and is given by the hydrostatic equation $P_1 = \rho g h + P_a$, where $g = 9.81\,\mathrm{m\,s^{-1}}$ is the gravitational acceleration at the Earth's surface, and P_a is the atmospheric pressure of the air above the water in the tube. In our setup, the second pressure $P_2 = P_a$, such that ΔP becomes simply $\Delta P = \rho g h$. As ρ and g are constant here, the pressure difference ΔP is controlled solely by h.

These conversions (of our dependent variable $\dot{m}$ to $\langle u \rangle$ and our independent variable h to ∇P, or $\Delta P/L$) mean that Eq. (1) can be solved explicitly as a function of the outputs from the experiment. In Fig. 4(b), we show the results we obtained for sintered samples of different ϕ. Equation (1) then relates the $\langle u \rangle$ to ΔP via a constant $\mu = 10^{-3}$ Pa s (water at 20 °C) and an unknown k. We use a few lines of code written in open-source Python™ to fit for that unknown k for each sample in Fig. 4(b) and to output the uncertainty on these fitted values (see Listing 1 in the supplementary material). However, a similar approach could easily be done by plotting the solution to Eq. (1) and adjusting k until it approximately matches the data. If the data deviate from Eq. (1) at high ΔP, then it may be that the flow had an additional inertial component and Eq. (2) should be used instead—however this is not dealt with here, and for the samples chosen here, Eq. (1) was valid.

VI. AN EXTRA STEP: USING A THEORETICAL PERMEABILITY MODEL

An important part of investigating physical phenomena is to compare empirical results with theoretical results. Here, we give the state-of-the-art theoretical result for the permeability of a sintered filter as a function of its total porosity and material properties. A sintering system of particles has been shown to have a permeability similar to that of the space between any domain of randomly placed freely overlapping spheres.[13,15] The permeability for random distributions of freely overlapping spheres is given by k_s, which in turn can be used to calculate k,

$$k_s = \frac{2(1-(\phi-\phi_c))}{s^2}, \qquad k = k_s(\phi-\phi_c)^b, \tag{3}$$

where ϕ_c is a critical porosity at which the system transitions from being permeable at $\phi > \phi_c$ to impermeable at $\phi < \phi_c$, s is the specific internal surface area of the pore network, and b is the percolation exponent. The values $\phi_c = 0.03$ and $b = 4.4$ are dimensionless and universal for systems of spherical sintering particles.[14,16]

Commercially available samples come with a defined value of s. Otherwise, it must be measured or predicted. Predicting s in sintered samples requires knowledge of the starting particle size from which the sintered sample was made, $\langle R \rangle$. If the sample is initially granular and monodisperse (i.e., glass beads prior to sintering), then $s = 3\phi/\langle R \rangle$. However, for sintered samples, the internal surface area is smoothed out during sintering and it is more effective to use a model for s that relies on the internal pore size, $\langle a \rangle$, rather than $\langle R \rangle$. The calculation for s is then for overlapping spheres[17]

$$s = \frac{(1-\phi)\ln(1-\phi)}{\langle a \rangle}, \tag{4}$$

and in the supplementary material, we provide a short code written in Python™ to compute $\langle a \rangle$ from $\langle R \rangle$ based on theory for random heterogeneous microstructures.[17]

In Fig. 5(a), we show that Eq. (3) is an excellent predictor of our experimental results without any adjustable parameters. If we define a dimensionless permeability $\overline{k} = k/k_s$, we can rearrange Eq. (3) as $\overline{k} = (\phi - \phi_c)^b$ to provide a universal dimensionless plot (Fig. 5(b)).

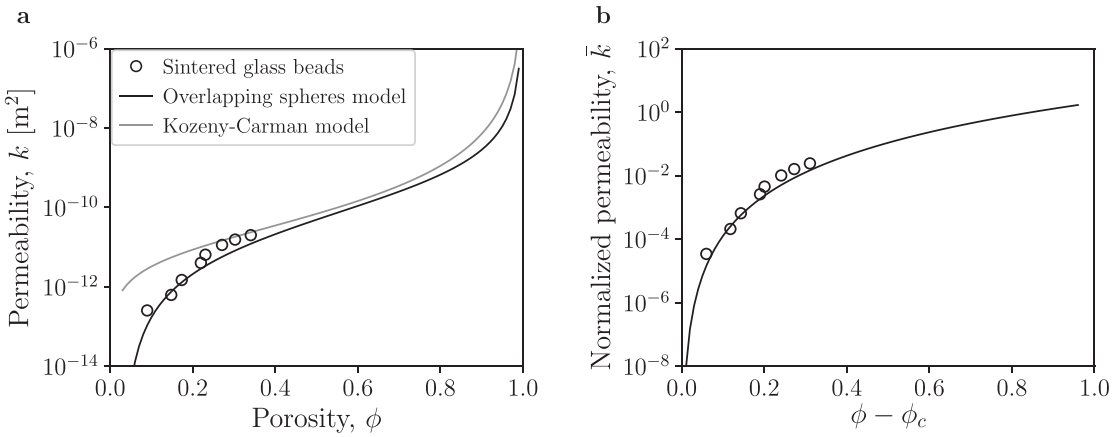

Fig. 5. (a) The permeability determined using Darcy's law (Eq. (1)) as a function of the total porosity. The solid black curves represent the theoretical results for a porous solid sintered material using monodisperse particle sizes $\langle R \rangle = 9.41 \times 10^{-5}$ m (glass beads) and a critical percolation threshold porosity of $\phi_c = 0.03$ [from previous work (Ref. 14)]. For comparison, the Kozeny-Carman model (Ref. 18) is shown, which overestimates the permeability at low porosity. (b) The results from (a) scaled by the factor k_s (see Eq. (3)). Model results for overlapping spheres (in both panels) are given in the main text and in detail elsewhere (Ref. 5, 13, 15, 22).

Finally, students could compare their data against other formulations for the permeability of porous media such as the widely used Kozeny-Carman model,[5,18–20] which states $k = \phi^3/(2s^2)$. We find that this model is not a good predictor of our data (Fig. 5(a)). This model was derived for packs of spheres and not for sintering systems and is not expected to be a good predictor of fluid permeabilities in this case. This is because sintering causes motion of the glass bead surfaces and renders them non-spherical and interconnected.

ACKNOWLEDGMENTS

This classroom activity was developed as part of the Petrophysik (Petrophysics) MSc-level course in Earth Sciences developed by Bettina Scheu and Fabian Wadsworth and run since 2014, which was supported by the Studi_forscht@GEO program at the Ludwig-Maximilians-Universität (Grant Nos. W16_F18 and W16_F6). The authors are grateful to the students who have taken this course over the years for their enthusiasm and feedback in refining practical laboratory activities such as this. The authors thank Jérémie Vasseur for valuable assistance throughout and for helping technically to formulate the Listing items in the supplementary material. A similar exercise has recently been formulated by Jackie Kendrick and Anthony Lamur at the University of Liverpool (https://geohubliverpool.org.uk/resource/porosity-permeability/).

[a]Electronic mail: fabian.b.wadsworth@durham.ac.uk

[1]H. Darcy, *Les Fontaines Publiques de la Ville de Dijon (The Public Fountains of the City of Dijon)* (Hennuyer, Paris, 1856).
[2]G. J. Plain and H. L. Morrison, "Critical Reynolds number and flow permeability," Am. J. Phys. **22**, 143–146 (1954).
[3]S. Withaker, "The Forchheimer equation: A theoretical development," Transp. Porous Media **25**, 27–61 (1996).
[4]S. Torquato and B. Lu, "Rigorous bounds on the fluid permeability: Effect of polydispersivity in grain size," Phys. Fluids A **2**, 487–490 (1990).
[5]N. S. Martys, S. Torquato, and D. P. Bentz, "Universal scaling of fluid permeability for sphere packings," Phys. Rev. E **50**, 403 (1994).
[6]A. Nabovati, E. W. Llewellin, and A. C. M. Sousa, "A general model for the permeability of fibrous porous media based on fluid flow simulations using the lattice Boltzmann method," Compos., Part A **40**, 860–869 (2009).
[7]B. L. Krasnyi, V. P. Tarasovskii, A. Y. Val'dberg, and T. O. Kaznacheeva, "Porous permeable ceramics for filter elements cleaning hot gases from dust," Glass Ceram. **62**, 134–138 (2005).
[8]C. Klug and K. V. Cashman, "Permeability development in vesiculating magmas: Implications for fragmentation," Bull. Volcanol. **58**, 87–100 (1996).
[9]H. Bruus, *Theoretical Microfluidics* (Oxford U. P., Oxford, 2008), Vol. 18.
[10]C. Gianino, "Experimental analysis of the Italian coffee pot 'moka'," Am. J. Phys. **75**, 43–47 (2007).
[11]J. Wenner *et al.*, "The case for infusing quantitative literacy into introductory geoscience courses," Numeracy **2**, 4 (2009).
[12]F. Wadsworth *et al.*, "Trashcano: Developing a quantitative teaching tool to understand ballistics accelerated by explosive volcanic eruptions," Volcanica **1**, 107–126 (2018).
[13]F. B. Wadsworth *et al.*, "Topological inversions in coalescing granular media control fluid-flow regimes," Phys. Rev. E **96**, 033113 (2017).
[14]F. B. Wadsworth *et al.*, "Sintering of viscous droplets under surface tension," Proc. R. Soc. A **472**, 20150780 (2016).
[15]F. B. Wadsworth *et al.*, "Universal scaling of fluid permeability during volcanic welding and sediment diagenesis," Geology **44**, 219–222 (2016).
[16]B. I. Halperin, S. Feng, and P. N. Sen, "Differences between lattice and continuum percolation transport exponents," Phys. Rev. Lett. **54**, 2391–2394 (1985).
[17]S. Torquato, *Random Heterogeneous Materials: Microstructure and Macroscopic Properties* (Springer Science & Business Media, New York, 2013), Vol. 16.
[18]A. E. Scheidegger, *Physics of Flow through Porous Media. Physics of Flow through Porous Media* (University of Toronto, Toronto, 1963).
[19]P. C. Carman, "Fluid flow through granular beds," Chem. Eng. Res. Des. **75**, S32–S48 (1997).
[20]J. Kozeny, "Uber kapillare leitung der wasser in boden," Sitzungsber. Akad. Wiss. Wien. **136**, 271–306 (1927).
[21]F. Crameri, "Scientific colour-maps," available at <http://www.fabiocrameri.ch/colourmaps.php> (accessed July 8, 2019).
[22]J. Vasseur and F. B. Wadsworth, "Sphere models for pore geometry and fluid permeability in heterogeneous magmas," Bull. Volcanol. **79**, 77 (2017).
[23]See supplemental material at http://dx.doi.org/10.1119/10.0000296- for example datasets and example codes used in this article.